JOURNAL OF GUIDANCE, CONTROL, AND DYNAMICS
Vol. 25, No. 5, September–October 2002

Robust Individual Blade Control Algorithm for a Dissimilar Rotor

Beatrice Roget* and Inderjit Chopra†
University of Maryland, College Park, Maryland 20742

A new control methodology is formulated for vibration reduction at the rotor hub by controlling trailing-edge flaps. The novelty of the proposed methodology lies in its ability to control each rotor blade separately and optimally, taking into account blade-to-blade dissimilarities, while using exclusively fixed-frame measurements. The controller is formulated in the time domain and adaptively generates in real time individual control inputs to the trailing-edge flaps to achieve vibration reduction. Numerical simulations using a hingeless rotor model show that the controller generates control inputs to each blade, taking blade dissimilarities into account, and successfully minimizes hub vibrations.

Nomenclature

C_T/σ	=	blade loading
F	=	fixed-frame load
F_0	=	uncontrolled fixed-frame load
I_K	=	identity matrix of size, K
kN/rev	=	integer multiple of N times the rotor frequency
N	=	number of rotor blades
N_s	=	number of samples per revolution
R	=	rotor radius
S	=	permutation matrix
α	=	sectional angle of attack
δ	=	flap deflection angle
$\partial\alpha/\partial\delta$	=	flap effectiveness
μ	=	advance ratio
Ω	=	rotor revolutions per minute

Subscripts

k	=	blade number
n	=	iteration number

Introduction

THE modern helicopter is susceptible to excessive vibrations because of increased operational demands in terms of speed, maneuverability, agility, and crew effectiveness. A high level of vibration causes fatigue failure of critical components, seriously affects ride quality and system reliability, increases maintenance costs, and degrades equipment performance. Helicopter vibration has several sources, such as the main rotor, tail rotor, engine, transmission, and the rotor downwash on the fuselage. The main rotor, however, is the main source of helicopter vibration. The main rotor is routinely subjected to severe vibratory loads in forward flight due to the highly unsteady aerodynamic environment at the rotor disk and the cyclically varying rotor blade control pitch angles. These vibratory loads are transmitted to the fuselage via the rotor hub.

Traditionally, vibration reduction is achieved by such passive control methods as rotor and fuselage structural optimization and installation of vibration absorbers on critical components. These methods are associated with large weight penalties and have limited effectiveness away from the tuned flight condition. To improve these limitations, various approaches to active vibration control have been explored,[1] such as higher harmonic control (HHC), individual blade control (IBC), and active control of on-blade actuators, for example, trailing-edge flaps. Unlike the passive methods of vibration control, these active control schemes affect the vibratory loads at their source, before they propagate into the airframe.

For an N-bladed rotor with identical blades, only vibrations at harmonics that are integer multiples of N times the rotor frequency are transmitted through the rotor mast, due to cancellation of the other harmonics at the hub. The idea behind the HHC approach is to superimpose an N/rev excitation to the swashplate motion to control the helicopter, such that the resulting additional blade loads cancel the unsteady airloads responsible for the N/rev fixed-frame vibration. HHC is a proven technology and has been demonstrated through numerical simulation, model and full-scale rotor tests in wind tunnels, and flight tests of full-scale vehicles to reduce vibrations.[2–6] However, by using swashplate actuation, the frequency content of the blade pitch motion is restricted, and individual control of rotor blades is not possible. The ability to control each blade independently and without frequency restrictions is very important for stall alleviation and vibration control of a dissimilar rotor. Because blade-to-blade load dissimilarities are transmitted directly to the fixed frame, there is always some level of fuselage response at harmonics other than kN/rev. This problem is addressed by frequent rotor inspection and by manual blade tracking if required, by adjusting trailing-edge tabs in an iterative manner. This approach entails high operating and maintenance costs. In the conventional IBC approach, each blade pitch is controlled independently using blade root actuators in the rotating frame. This allows arbitrary blade pitch motions and the inclusion of blade tracking for improved vibration reduction. The effectiveness and potential for vibration reduction of IBC has been demonstrated analytically[7,8] and experimentally.[9,10] However, both HHC and IBC are associated with drawbacks such as high-power requirements, additional weights and complexity, and high pitch-link loads. With the development of smart structure materials, considerable effort is now being directed toward active control of on-blade actuators.[11,12] Potential advantages of this approach may be reduced weight penalty, low-power consumption, and enhanced airworthiness. Like conventional IBC, each blade actuator can be individually controlled over a wide range of frequencies. Several investigations have analytically demonstrated that active trailing-edge flaps can achieve a degree of vibration reduction comparable with conventional IBC while using moderate input angles.[13,14] Recently closed-loop wind tunnel tests on a four-bladed Mach scale rotor using piezobimorph-actuated trailing-edge flaps was conducted in the Glenn L. Martin wind tunnel. The performance of this actuator was successfully demonstrated to minimize 4/rev hub loads by over 90% for steady and transient flight conditions.[15]

Presented as Paper 2001-1433 at the AIAA/ASME/ASCE/AHS/ASC 42nd Structures, Structural Dynamics, and Materials Conference, Seattle, WA, 16–19 April 2001; received 28 August 2001; revision received 15 March 2002; accepted for publication 18 March 2002.

*Graduate Research Assistant, Department of Aerospace Engineering. Student Member AIAA.

†Alfred Gessow Professor and Director, Alfred Gessow Rotorcraft Center, Department of Aerospace Engineering. Fellow AIAA.

For a feedback system, controller methodology is needed to determine optimal control inputs to each blade. The majority of helicopter vibration reduction studies have been based on linear, quasi-static, frequency-domain representations of the transfer function of the helicopter response to control inputs. For adaptive control strategies, Kalman-filter-type identification of helicopter parameters has been normally used together with a quadratic cost-function-type controller to determine the optimal control harmonics for vibration alleviation.[16,17] In the present study, the controller formulation follows the conventional approach, but uses a time-domain representation of the helicopter vibration to avoid limiting the frequency content of both the inputs (fixed system vibratory loads) and outputs (individual blade control angles). This scheme is based on the work by Spencer et al.,[18–20] where the controller uses a single hidden layer neural network representation to reduce vibratory hub loads of an identical rotor.

In a real rotor, the vibration transmitted to the fuselage can be divided into two parts: the baseline vibration and the additional vibration caused by blade-to-blade dissimilarities in mass, stiffness, and aerodynamic properties. To achieve vibration reduction, both parts must be minimized. The first part corresponds to the vibration generated by an equivalent rotor with identical blades and hence contains exclusively kN/rev harmonics. Therefore, to reduce this vibration component, the blades can be controlled together; that is, a common control input is applied with the appropriate phase shift to all blades. In contrast, to reduce the second component of vibration, the blades should be controlled independently. As a result, for baseline vibration reduction, only fixed-frame measurements are adequate, whereas for other vibrations, measurements containing individual information from each blade are required. Hence, rotating-frame measurements may be needed. Fixed-system hub shears and moments cannot be measured directly, but they can be accurately derived from a series of shaft bending strain gauges (balance). Hub vibrations can also be monitored using accelerometers. Modern micromechanical sensors based on piezoelectric and optical technologies are able to detect very small changes in vibration, of the order of $10^{-6}g$ (Ref. 21). On the other hand, acquiring sensor data from each rotor blade is difficult and involved. Rotor blade instrumentation systems must operate in a severe dynamic environment, where the centrifugal load may range up to $900g$ at the rotor blade tip and vibratory load spectrum can extend past 60 Hz (Refs. 22 and 23). Therefore, only limited measurements, such as blade root flapping and pitching moments, can be conveniently acquired in the rotating frame using on-blade strain gauges. Because of these difficulties, existing control schemes designed for helicopter vibration reduction are based on fixed-frame measurements and assume tracked rotor systems with identical blades, resulting in degraded performance when the algorithm is applied to a rotor with blade-to-blade dissimilarities.[24]

The objective of this research is to develop a refined time-domain control methodology and to demonstrate numerically that complete vibration reduction can be achieved in helicopters with on-blade actuators, by generating individual optimal control inputs to each blade while using exclusively fixed-system measurements.

The paper is organized as follows. First, the simulation model of the helicopter rotor with a trailing-edge flap is presented. Next, the new control methodology (individual flap control) is discussed in detail. Finally, sample calculations for a few test cases are presented and discussed.

Mathematical Model of Rotor System

The helicopter is represented by a nonlinear model of N elastic blades. Only the flap bending motion is considered. Governing equations are derived using a generalized Hamilton's principle applicable to nonconservative systems:

$$\delta\Pi = \int_{\Psi_1}^{\Psi_2} (\delta U - \delta T - \delta W)\,\mathrm{d}t$$

$$= \int_{\Psi_i}^{\Psi_f} \sum_{i=1}^{N} (\delta U_i - \delta T_i - \delta W_i)\,\mathrm{d}\Psi = 0 \tag{1}$$

where δU is the virtual variation of strain energy and δT is the virtual variation of kinetic energy. External aerodynamic forces on the rotor blade contribute to the virtual work variation δW. The trailing-edge flap effect is represented in the corresponding segment of each blade k by an additional term in the sectional angle of attack:

$$\alpha_k^{(\mathrm{TEF})} = \alpha_k^{(\mathrm{noTEF})} + \frac{\partial\alpha}{\partial\delta}\delta_k \tag{2}$$

$\partial\alpha/\partial\delta$ is the rate of change of effective angle of attack with flap deflection. For this analysis, the unsteady aerodynamic effects of the trailing-edge flap are not represented. Finite element methodology is used to discretize the governing equations of motion and allows easy adaptation for nonuniform blade properties.

The first step in the aeroelastic analysis procedure is to trim the vehicle for the specified operating condition. Trim involves the calculation of rotor controls, vehicle orientation, and blade response such that the vehicle trim equations and the blade periodic response equations are solved simultaneously. Satisfaction of the vehicle trim equations implies that the resultant forces and moments on the vehicle, averaged over one rotor revolution, become zero. The blade finite element equations are transformed to normal mode space for efficient solution of the blade response. The nonlinear, periodic, normal mode equations are then solved for steady response using a finite element in time method. Steady and vibratory components of the rotating frame blade loads are calculated using the force summation method. In this approach, blade aerodynamic and inertia forces are integrated directly over the length of the blade. Fixed-frame hub loads are calculated by summing the contributions of individual blades. The coupled trim procedure is then carried out to solve for the blade response, pilot input trim control angles, and vehicle orientation simultaneously.

Once a trim solution has been calculated for the baseline rotor at a specified flight condition, dissimilarities are simulated between the blades. The periodic (out-of-trim) solution is obtained for each blade, and the controller is activated. The resulting transient blade response is then calculated for one rotor revolution by integrating the normal mode equations in time. The time integration is based on the Runge–Kutta explicit scheme. For the first rotor revolution, the excitation is random, and the periodic solution provides the initial condition. For subsequent rotor revolutions, the initial condition is taken from the previous transient solution. These calculations are carried out for each blade independently to account for blade dissimilarities. The transient blade response is obtained for three rotor revolutions, but only the last revolution, which is close to periodic response, is used in the adaptive controller. From the blade response, the transient rotating frame loads are calculated. Contributions from each blade are then summed to calculate the fixed frame vibratory shears and moments to be minimized. This procedure is shown in Fig. 1.

Individual Flap Control Methodology

This control scheme is developed herein to achieve vibration reduction in the special case when the rotor blades have dissimilarities, resulting in non-kN/rev harmonics in the fixed-frame hub vibratory loads. This scheme is a refined version of a previous work by the present authors.[24] In theory, reduction of fixed-system vibratory loads can be achieved by using the same control inputs to all blades with the appropriate phase. However, when the rotor is dissimilar, the required trailing-edge flap deflection angles for minimization may become too large.[24] Because some degree of rotor dissimilarity is always present, it may be important to control each trailing-edge flap individually.

To control the blades independently, it may be necessary to obtain individual information from each blade. In view of the complexities associated with acquiring rotating-frame data, the present control scheme is designed to use exclusively fixed-frame measurements to extract individual blade information. To this effect, different control inputs are applied to each blade, as shown in Fig. 1. It is then possible to extract individual blade information from the knowledge of the fixed-frame load measurements and the individual flap control inputs, explained as follows.

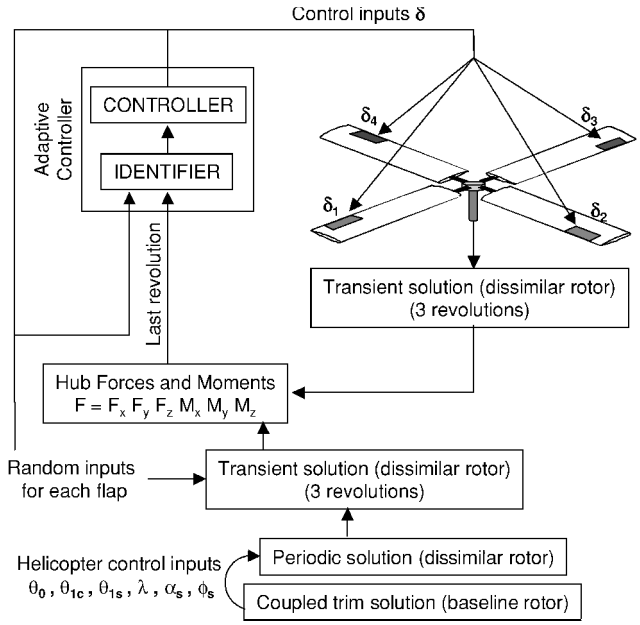

Fig. 1 Individual flap control scheme block diagram.

For a four-bladed rotor, assuming the system is linear and periodic, the relationship between control inputs and fixed frame load can be written as

$$\boldsymbol{F} = \boldsymbol{F}_0 + [T_1 \;\; T_2 \;\; T_3 \;\; T_4] \cdot \begin{Bmatrix} \boldsymbol{\delta}_1 \\ \boldsymbol{\delta}_2 \\ \boldsymbol{\delta}_3 \\ \boldsymbol{\delta}_4 \end{Bmatrix} = \boldsymbol{F}_0 + [T] \cdot \{\boldsymbol{\delta}\} \tag{3}$$

where T_k are the transfer matrices relating the sampled vibration to the sampled controls, δ_k are the individual flap controls, F is the total fixed-frame vibration, and F_0 is the uncontrolled fixed-frame vibration, sampled at N_s points over one rotor revolution. In the case of perfectly identical blades, there exists a relationship between the transfer matrices T_k and T_{k+1},

$$T_{k+1} = S \cdot T_k \tag{4}$$

where S is a matrix that operates a permutation on the transfer matrix rows,

$$S = \begin{bmatrix} 0 & I_p \\ I_q & 0 \end{bmatrix} \tag{5}$$

where $p = (N-1)(N_s/N)$ and $q = N_s/N$.

Note that, in expression (3), the only assumptions made are periodicity and linearity. The system is not assumed to be time invariant. The transfer matrices T_k for each blade are unknown a priori; hence, a system identification technique is needed. In this paper, we use the classic Kalman filter method to identify the transfer matrices. Although the uncontrolled vibration can be obtained from measurements (when no controls are applied), F_0 should also be estimated online because it will vary when flight conditions or helicopter characteristics change. Equation (3) can then be rewritten as

$$\boldsymbol{F} = [T \quad \boldsymbol{F}_0] \cdot \begin{Bmatrix} \boldsymbol{\delta} \\ 1 \end{Bmatrix} \tag{6}$$

At iteration n, the measurement vector is $\boldsymbol{Z}_n = F$, and the state matrix to be estimated is $X_n = [T \;\; F_0]$. The Kalman filter approach obtains an estimate of X_n, which minimizes the errors produced between the measured output and the output predicted using the estimate of X_n and the input. This is done for each row of expression (6).

In Eq. (3), it is assumed that the steady-state periodic solution is reached. The load vectors are sampled over one rotor revolution; therefore, the system model is static. The system model is written as

$$X_n = X_{n-1} + W_{n-1} \tag{7}$$

where W_n is the system noise matrix. Each line of W_n is assumed to be a zero-mean, white sequence of constant covariance Q.

The measurement model comes from Eq. (6):

$$\boldsymbol{Z}_n = X_n \cdot \boldsymbol{H}_n^T + \boldsymbol{V}_n, \qquad \boldsymbol{H}_n = [\boldsymbol{\delta}^T \quad 1] \tag{8}$$

where H_n is the measurement matrix and V_n is the measurement noise, also assumed to be a zero-mean, white sequence. The elements of V_n are assumed to have the same covariance R, assumed constant. To begin the system identification procedure, a value is chosen for the system noise covariance matrix Q and the measurement noise covariance R (scalar). Initial guesses are also made for the initial state matrix X_0 and estimate error covariance matrix P_0.

The system identification procedure is then carried out, using the discrete Kalman filter equations: the Kalman gain matrix,

$$K_n = P_{n-1}\boldsymbol{H}_n^T \left[\boldsymbol{H}_n P_{n-1} \boldsymbol{H}_n^T + R\right]^{-1} \tag{9}$$

the error covariance update,

$$P_n = [I - K_n \boldsymbol{H}_n] \cdot [P_{n-1} + Q] \tag{10}$$

and the state estimate update,

$$X_n = X_{n-1} + \left\{\boldsymbol{Z}_n - X_{n-1}\boldsymbol{H}_n^T\right\} \cdot \left\{\boldsymbol{K}_n^T\right\} \tag{11}$$

Note that the computation of the Kalman gain matrix only requires inversion of a scalar. Based on the computed parameter estimates, a deterministic control law is required to generate individual optimal control inputs for each trailing-edge flap.

To minimize the resulting fixed-frame load, each trailing-edge flap k must produce a load L_k in the rotating frame such that

$$\sum_{k=1}^{N} \boldsymbol{L}_k = -\{\boldsymbol{F}_0 - (\boldsymbol{F}_0)_{\text{mean}}\} \tag{12}$$

so that when the individual controls are applied simultaneously, in the ideal case, the vertical hub load is constant and equal to the trimmed value

$$\boldsymbol{F} = \boldsymbol{F}_0 + \sum_{k=1}^{N} \boldsymbol{L}_k = (\boldsymbol{F}_0)_{\text{mean}} \tag{13}$$

From Eq. (12), it is clear that there exists several ways to generate the optimal control inputs for each blade. In Ref. 24, three constraints were imposed to guide the choice of the optimal control inputs:

1) All blades should contribute to the same level in the reduction of the kN/rev fixed-frame load ($k > 1$).

2) The more a blade is different from the average blade, the more it should contribute to the reduction of the other harmonics of the fixed-frame load.

3) If two blades are identical, they should receive identical control inputs.

These constraints allowed us to define an objective function to be minimized for each blade. The controller performance achieved for the vertical hub load alone was very good (99% reduction in 150 revolutions without noise). However, these constraints were found to be too limiting in the case of multiple loads control, leading to less vibration reduction. Therefore, in this paper, we adopt a more general control law, which does not impose any constraints on the control inputs. The deterministic control law is based on the minimization of the quadratic performance index J:

$$J = \boldsymbol{Y}^T W_F \boldsymbol{Y} + \boldsymbol{\delta}^T W_\delta \boldsymbol{\delta} + (\boldsymbol{\Delta\delta})^T W_{\Delta\delta} (\boldsymbol{\Delta\delta}) \tag{14}$$

where $Y = F - (F_0)_{\text{mean}}$.

The weighting matrices W_F, W_δ, and $W_{\Delta\delta}$, applied to the vibrations, control, and rate of change of control, respectively, may be

changed to modify the relative importance of these various components. The optimal control input is determined by putting the partial derivative of J with respect to δ equal to zero:

$$\frac{\partial J}{\partial \boldsymbol{\delta}} = \{\mathbf{0}\} \tag{15}$$

Thus at each iteration n,

$$(\boldsymbol{\delta}^{\text{opt}})_n = D \cdot \left\lfloor W_{\Delta\delta}(\boldsymbol{\delta}^{\text{opt}})_{n-1} - T^T W_z \mathbf{Y}_n \right\rfloor$$

$$D = \left(T^T W_z T + W_{\Delta\delta} + W_\delta\right)^{-1} \tag{16}$$

Note that because the same performance index is used for all blades, the vector $\boldsymbol{\delta}^{\text{opt}}$ gives directly the optimal control angles for each trailing-edge flap. For a four-bladed rotor,

$$\boldsymbol{\delta}^{\text{opt}} = \left\{\delta_1^{\text{opt}} \quad \delta_2^{\text{opt}} \quad \delta_3^{\text{opt}} \quad \delta_4^{\text{opt}}\right\}^T \tag{17}$$

The control law is extended to allow control of multiple loads in the fixed frame. The performance index to be minimized is written for N_l loads to be controlled:

$$J = \sum_{nl=1}^{N_l} \left(\mathbf{Y}^T W_F \mathbf{Y}\right)_{nl} + \boldsymbol{\delta}^T W_\delta \boldsymbol{\delta} + (\Delta\boldsymbol{\delta})^T W_{\Delta\delta}(\Delta\boldsymbol{\delta}) \tag{18}$$

where $(\mathbf{Y})_{nl} = [\mathbf{F} - (\mathbf{F}_0)_{\text{mean}}]_{nl}$.

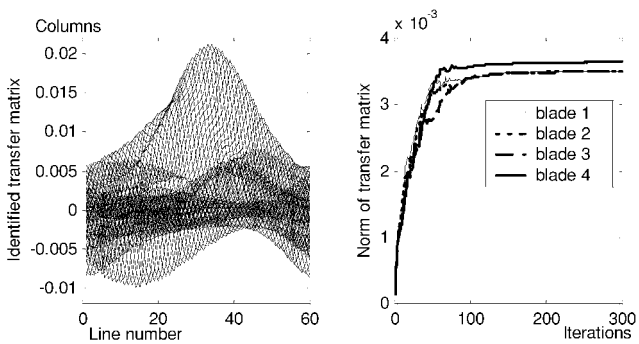

a) Open-loop identification

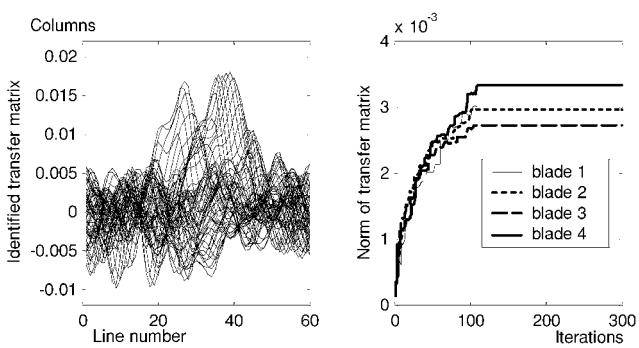

b) Original closed-loop identification

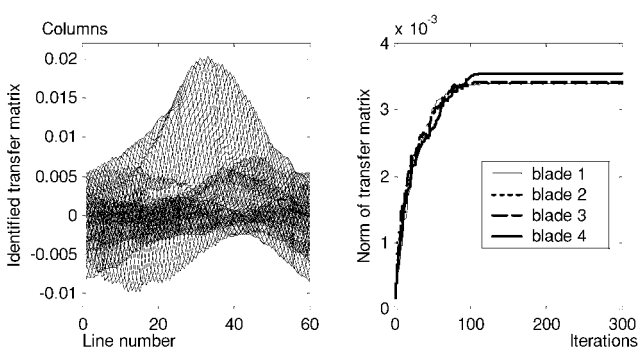

c) Modified closed-loop identification

Fig. 2 Open-loop and closed-loop identification.

When this procedure is used, the controller is able to generate individual control inputs to each trailing-edge flap, using only measurements in the fixed system.

Closed-Loop Identification Problem

Closed-loop and open-loop system identification performance may differ significantly. During open-loop identification, random excitation of the system ensures that the system will always generate diverse enough outputs for correct identification. In closed-loop identification, however, the control commands are chosen to minimize helicopter vibration. As the controller approaches a steady-state optimal control solution, the control commands from one step to the next will not be very different because they are nearly optimal. In this situation, the identified parameters can prematurely converge to values different from the real solution. Another problem can arise when the measurements are contaminated with noise. As the controller reduces the vibration, the stage may be reached where the noise begins to dominate the residual measured vibration signals. The system identification algorithm may, therefore, erroneously attempt to identify a matrix relating the small changes in control to the random changes in the measurement signal. Note that, in some cases, vibration could be well controlled even with a poorly identified transfer matrix. However, in other cases, a poor identification could result in a totally degraded controller performance; hence, it becomes necessary to improve the closed-loop identification process.

To improve the closed-loop control performance, random input angles of small amplitude are added to the computed optimal control

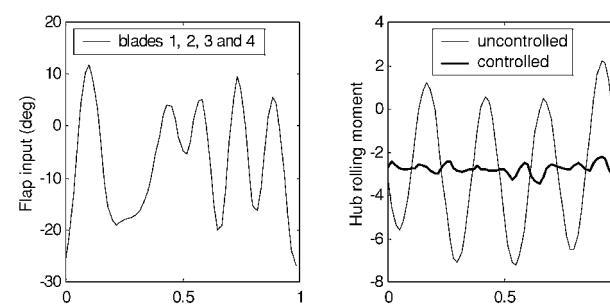

a) Collective flap control

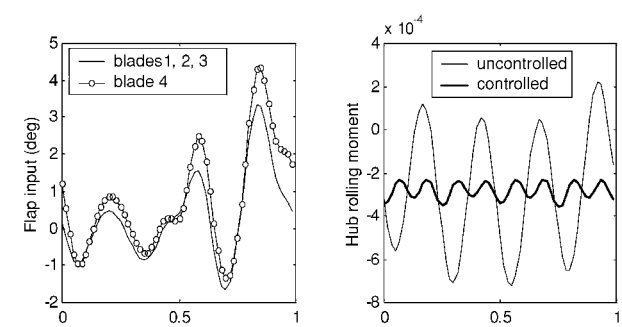

b) Individual flap control with restricted inputs

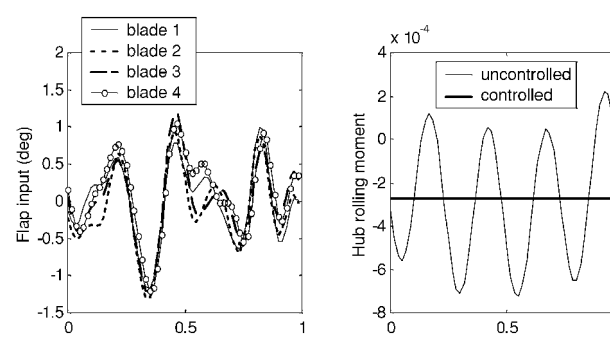

c) Individual flap control with unrestricted inputs

Fig. 3 Performance of different flap control methodologies for hub rolling moment control.

inputs when the identified parameters approach their converged value. An index is defined to quantify the parameter identification convergence, for each blade k, at iteration n:

$$\left(J_k^{\text{conv}}\right)_n = \frac{1}{N_s^2}\sum_{i=1}^{N_s}\sum_{j=1}^{N_s}|T(i,j)|_n - |T(i,j)|_{n-1} \qquad (19)$$

When the convergence index for each blade becomes small enough, the computed optimal inputs for each flap are applied without additional input.

With this method used, the results are presented for open-loop identification (Fig. 2a), original closed-loop identification (Fig. 2b), and modified closed-loop identification (Fig. 2c). These results are obtained for a dissimilar rotor. The mass of blade 4 is increased uniformly by 1%, whereas the mass of other blades is kept at the baseline value. The left-hand sides of Figs. 2a–2c show representations of the identified transfer matrix for blade 1 (T_1), after convergence. The matrix columns are plotted vs the line number, and the matrix size is $N_s = 60$. The right-hand sides of Figs. 2a–2c show the time history of the norm of the identified transfer matrices for each blade. This norm is defined as

$$|T_k| = \frac{1}{N_s}\sum_{i=1}^{N_s}\sum_{j=1}^{N_s}|T_k(i,j)| \qquad (20)$$

During open-loop identification (Fig. 2a), the inputs are random, ensuring that the transfer matrices converge to the correct values. It is verified that the norm of the transfer matrix corresponding to the identical blades 1, 2, and 3 is equal, whereas it is different for blade 4. The relationship between T_1, T_2, and T_3 [Eq. (4)] is also verified. Figure 2a also shows that the system is not time invariant: For a time invariant system, each column of T_k is a permutation of the first column, so that the columns have the same amplitude.

Figure 2b shows the original closed-loop identification. The identified transfer matrix after convergence is very different than the open-loop identified matrix. This is because convergence is reached too early, at iteration 110, when the control inputs converge. In this case, the final transfer matrix norms are different for all four blades.

Finally, Fig. 2c shows the closed-loop identification, with the modified scheme. It is seen that adding small random angles to control inputs before convergence improves the transfer matrix identification, which becomes similar to the open-loop case. The benefit of this system-probing method on the identification performance is quite apparent in Fig. 2. However, in this case, the controller performance is not improved significantly: Even with the poorly identified transfer matrix from Fig. 2b, vibration is completely canceled after convergence of the control algorithm.

Sample Calculations

Results are obtained for a four-bladed hingeless rotor model. Each rotor blade is modeled using 10 spatial finite elements along the blade span. Five rotating natural flap modes for each blade are used for modal analysis. Eight time finite elements with fourth-order shape functions are used along the azimuth to calculate the blade response. When these values are used, a converged blade solution is obtained. The blade first rotating flap frequency is 1.11/rev.

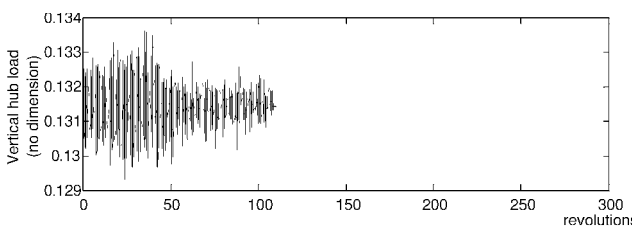

a) Vertical hub load time history

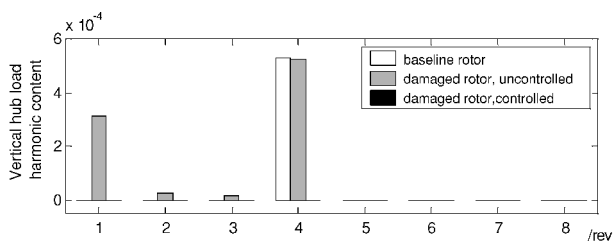

b) Harmonic content of vertical shear

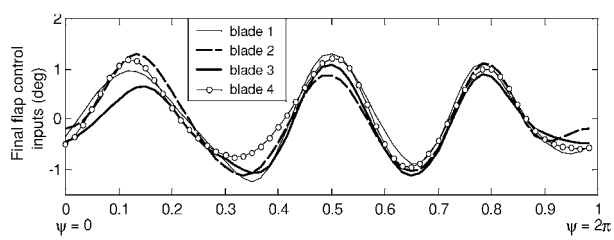

c) Optimal flap angles

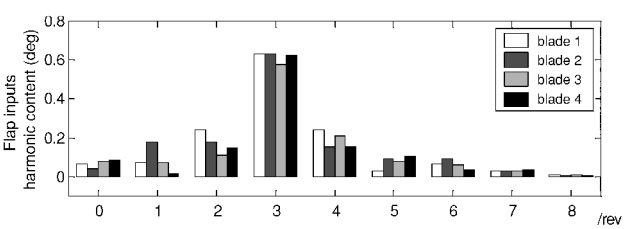

d) Harmonic content of flap angles

Fig. 4 Moisture absorption damage.

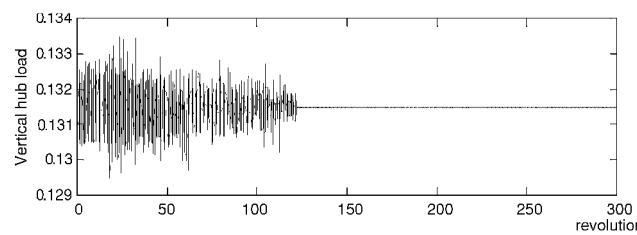

a) Vertical hub load time history

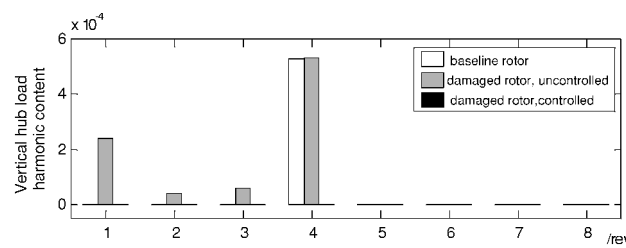

b) Harmonic content of vertical shear

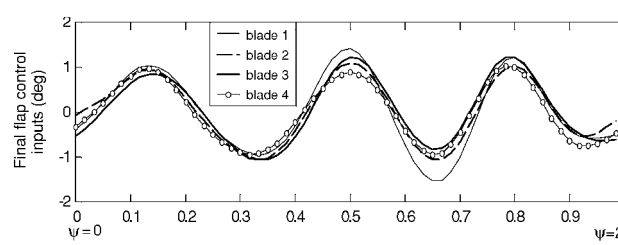

c) Optimal flap angles

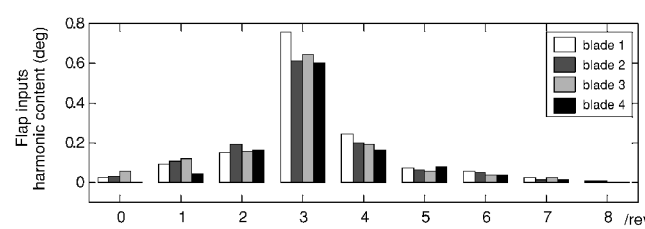

d) Harmonic content of flap angles

Fig. 5 Loss of trim mass damage.

The trailing-edge flap size is 20% of the blade chord and 18% of the radius in length, centered at $0.83R$. This corresponds to $\partial\alpha/\partial\delta = 0.50$, where $\partial\alpha/\partial\delta$ is the rate of change of effective angle of attack due to flap input.[25] A maximum flap input limit of ± 5 deg is imposed. Level flight conditions corresponding to $\mu = 0.30$ and $C_T/\sigma = 0.07$ are considered. The controller parameters are $W_F = 1$, $W_\delta = 2.5e{-}4$, and $W_{\Delta\delta} = 5e{-}6$. This set of controller parameters results in satisfying convergence properties and transient dynamics, but can be modified without deteriorating the controller performance. For measuring loads and to generate flap control inputs, 60 sample points per rotor revolution are used. To start the initial control iteration, small random flap angles are used as control inputs. As the controller adapts, the rate of change of the flap control inputs are restricted to avoid high transient loads at the hub.

The objective of the controller is to minimize oscillations in the vertical hub shear force, a key component that causes vibration at the pilot seat. All loads are nondimensionalized with respect to a reference force defined as $m_0(\Omega R)^2$, where m_0 is the mass per unit length of an equivalent uniform blade with the same flap inertia and ΩR is the blade tip speed. For each case, the helicopter rotor is first trimmed at the specified flight condition. The baseline vertical hub vibration is determined, and the controller is activated.

To simulate rotor dissimilarities among the four blades, one blade is assumed to contain a fault and the other blades are kept identical. The fault modeling approach is based on that of Ganguli et al.[26] Four types of rotor dissimilarities are simulated: 1) moisture absorption, 2) loss of trim mass, 3) damaged trailing-edge flap, and 4) bending stiffness damage.

Moisture absorption in a blade can occur in a humid environment and results in changes in the blade mass properties. To simulate this damage, the mass of the damaged blade is increased uniformly along the elastic axis by 3%. The masses of the other blades are kept fixed at the baseline value. Loss of trim mass is modeled by removing 5% of baseline mass from a particular section of a rotor blade. This section is chosen between 94 and 95% of the blade span. To simulate a damaged trailing-edge flap, it is assumed that the damaged flap has a steady 0.1-deg deflection angle in the uncontrolled state compared to zero deflection angles of the undamaged flaps. Therefore, the damaged blade has additional lift at the tip, causing an out-of-track condition. The stiffness damage is modeled by reducing the bending stiffness of a particular section of the blade to 85% of the baseline value. This section extends from the root to 10% of the rotor radius. Finally, the controller behavior in the case of a real dissimilar rotor is studied. In this case, some inherent damages or unbalances are present. This is simulated by randomly introducing differences in each blade mass and stiffness properties within 5% of the baseline properties.

Figure 3 shows the performance of different flap control methodologies for the reduction of the hub rolling moment, with moisture absorption damage in blade 4. The left-hand sides of Figs. 3a–3c represent the optimal flap inputs for all blades, whereas the right-hand sides show the hub rolling moment, both before and after control. To obtain Figs. 3a, the collective flap control method is used, where the same phase-shifted flap input is applied to all blades. Figures 3b correspond to the individual flap control with restricted inputs: Different

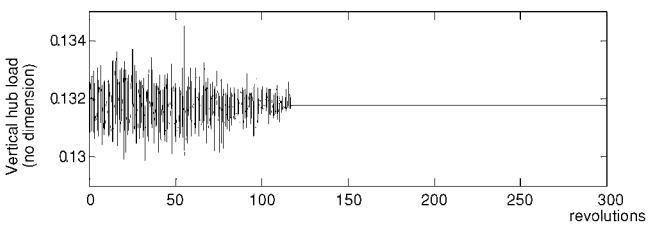

a) Vertical hub load time history

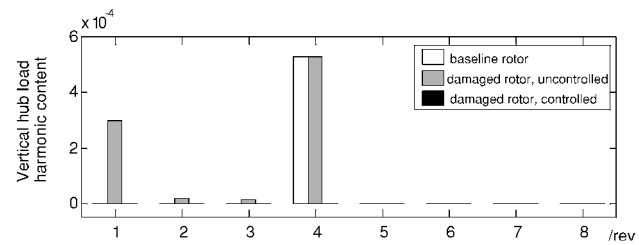

b) Harmonic content of vertical shear

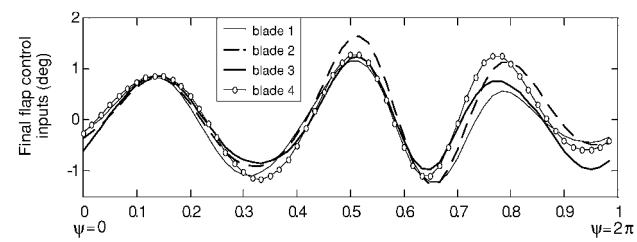

c) Optimal flap angles

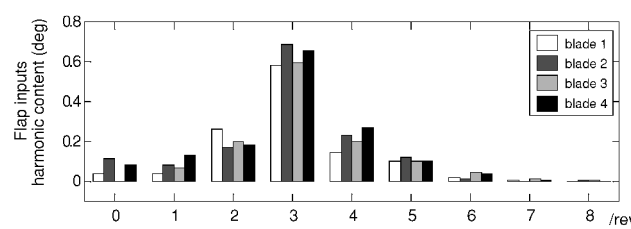

d) Harmonic content of flap angles

Fig. 6 Damaged trailing-edge flap.

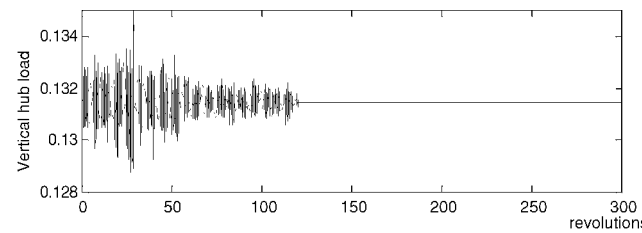

a) Vertical hub load time history

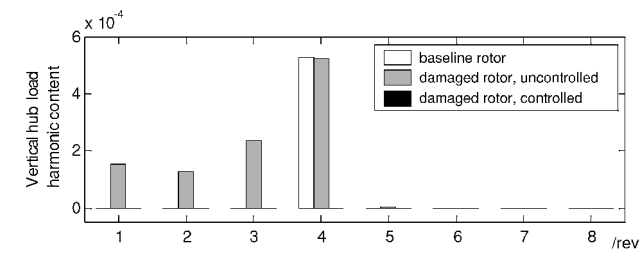

b) Harmonic content of vertical shear

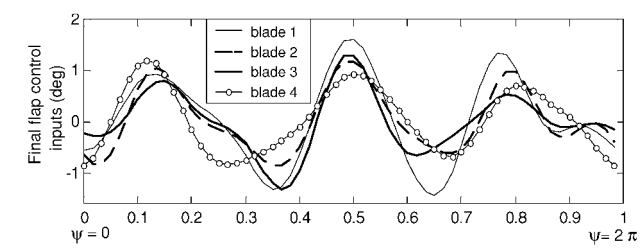

c) Optimal flap angles

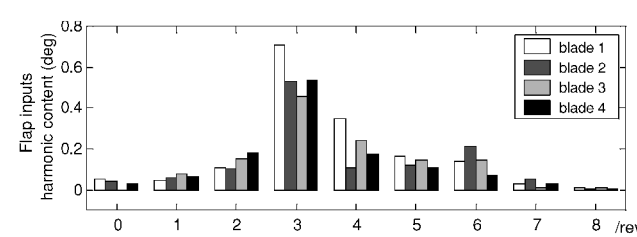

d) Harmonic content of flap angles

Fig. 7 Bending stiffness damage.

flap inputs are applied to different blades; however, identical flap inputs are applied to blades that are identical. Finally, Figs. 3c are obtained using the present flap control methodology, without any restriction for the flap inputs. The predicted flap amplitudes for the collective flap control are impractical (−25–12 deg). This can be explained by dividing the required flap input into two parts: One part is necessary for reducing the 4/rev vibration (kN/rev); another part is required to cancel the effect of the dissimilarities (non-kN/rev). With the first control method, the 4/rev component can be canceled using a flap input of relatively small amplitude (±1.5 deg). However, it is very difficult to cancel the effect of the damage in blade 4 using the same input for all blades: The required flap input is extremely high (−25–12 deg). A similar observation was made from the recent model rotor test in the wind tunnel to minimize vibratory hub loads with bimorph-actuated flaps. With rotor dissimilarities, the flap requirements became excessive, resulting in the saturation of actuators and enormously degraded control performance.[27] With the second control method, individual flap control with restricted inputs, the required flap amplitude is reduced (−1.7–4.5 deg). However, only 80% vibration reduction is achieved. The vibration reduction achieved with the present control methodology is more than 99%. At the same time, the required flap angles are only ±1.3 deg in amplitude. Small flap angles get translated into a low actuation power for vibration minimization. Thus, Fig. 3 clearly illustrates the advantage of the present control methodology.

Figures 4–7 show the controller performance with a fault in blade 4 to minimize the vertical fixed-frame vibratory hub shear. Figure 8 shows the controller performance with a fault in all blades. Figures 4a–8a show the time history of the vertical hub shear. In all fault cases, this load is reduced completely (by more than 99%) in less than 120 rotor revolutions. In Fig. 4b–8b, the harmonic content of the vertical hub load is shown, for the baseline rotor with controller off, the damaged rotor with controller off, and the damaged rotor with the controller on. For the baseline rotor with identical blades, only 4/rev fixed-system loads are present. It is seen that most faults introduce a significant 1/rev component and smaller 2/rev and 3/rev components. The bending stiffness damage effect is more significant on the 3/rev component (Fig. 7b). Apparently, damage does not introduce any hub load harmonic above 4/rev using this simple rotor model. As shown in Figs. 4c–8c, the controller generates dissimilar flap angles for all blades, and the dominant harmonic component of these inputs is 3/rev (Figs. 4d–8d). The flap deflections required for each blade do not exceed 3 deg peak-to-peak for all damage cases. Note that even though damage is incorporated in one blade (blade 4), the flap input to each blade is somewhat different. Also note that even though there are negligible load harmonics above 4/rev, the controller seems to require small flap inputs at 6/rev and higher. Because these higher harmonic inputs may be more difficult to implement and may not be too significant for vibration reduction, it may be possible to neglect these without any major effect on the controller performance.

Figure 9 shows the controller performance when simultaneous reduction of several fixed-frame loads is attempted. In this case, the vertical hub shear and the pitching moment and rolling moment vibrations are reduced simultaneously, with equal weights: $W_{Fz} = W_{My} = W_{Mx} = 1$. All three loads are reduced by 99% after 150 rotor revolutions. As expected, the amplitude of the required flap

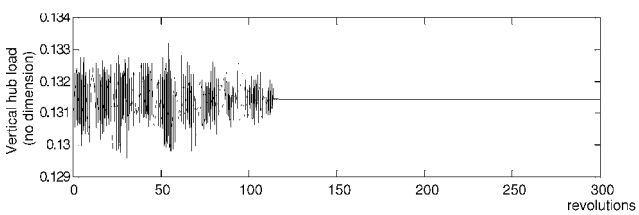

a) Vertical hub load time history

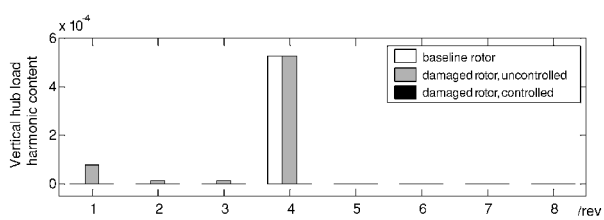

b) Harmonic content of vertical shear

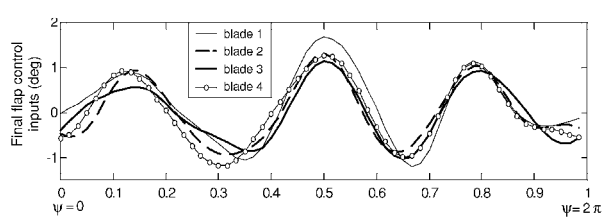

c) Optimal flap angles

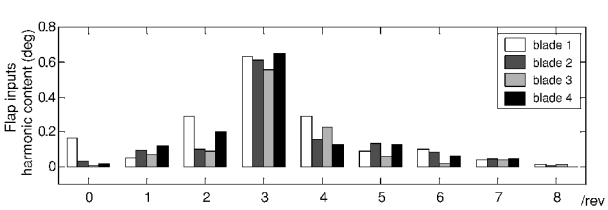

d) Harmonic content of flap angles

Fig. 8 Various damages in blade mass and stiffness.

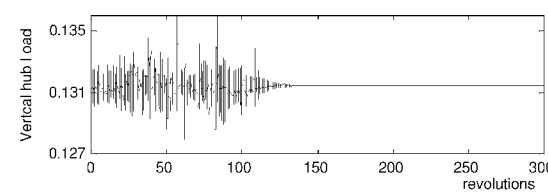

Vertical hub load

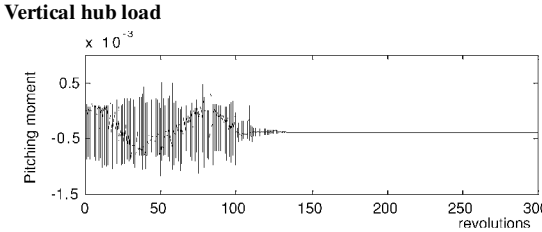

Hub pitching moment

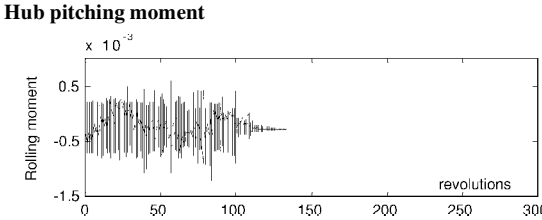

Hub rolling moment

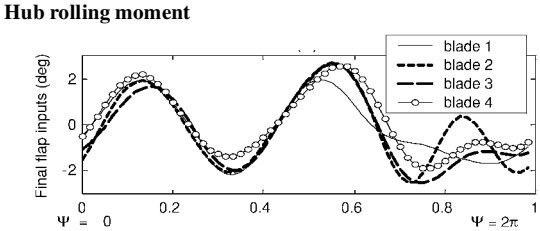

Optimal flap angles

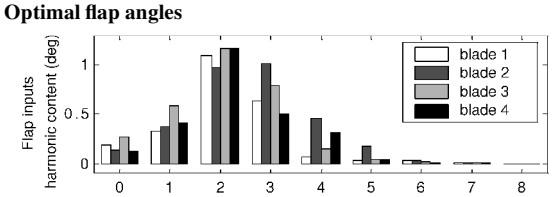

Harmonic content of flap inputs

Fig. 9 Multiple loads control with moisture absorption in blade 4.

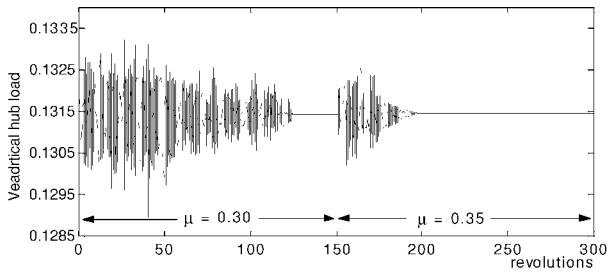

a) Vertical hub shear time history

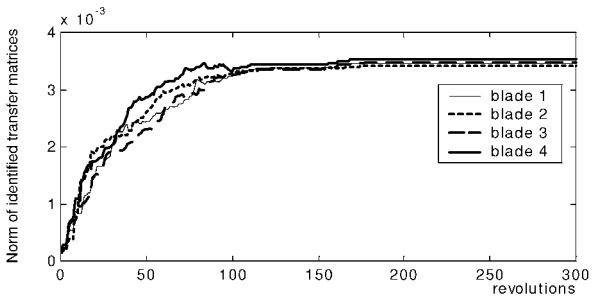

b) Time history of the identified transfer matrices norm

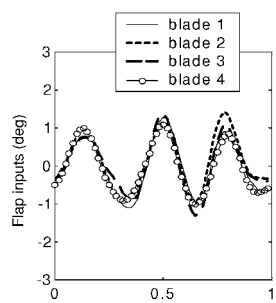

c) Optimal flap angles before advance ratio change, iteration 145, $\mu = 0.30$

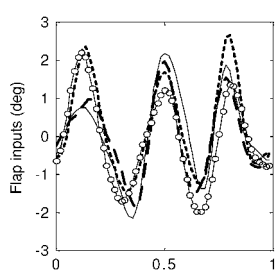

d) Optimal flap angles after advance ratio change, iteration 295, $\mu = 0.35$

Fig. 10 Effect of a change in advance ratio at iteration 150.

inputs is increased compared to the single load control. However, the flap amplitude remains realistic (less than ±3 deg).

Figure 10 shows the effect of a change in flight condition on the controller performance. This is shown for the moisture absorption damage in blade 4. The advance ratio is suddenly increased at iteration 150 from 0.3 to 0.35. Figure 10a shows that this sudden change results in increased vibration. However, the controller is able to identify the new transfer matrices and cancel vibration in about 50 revolutions. The identification of the new transfer matrices is apparent in Fig. 10b. The control angles required for the new flight condition are larger in amplitude: about ±2.5-deg amplitude for $\mu = 0.35$, compared to less than ±1.5 deg for $\mu = 0.3$ (Fig. 10c). Note that some vertical hub load time histories show substantial transients during controller identification. This problem can be alleviated by applying tighter constraints on the flap inputs (increasing W_δ or fixing a limit to the maximum increase in flap deflection in each iteration), but this also increases the controller learning period.

All of the preceding results have been obtained using computed clean hub loads (with no measurement error). To make the simulations more realistic, noise is added to the numerical predictions. The results are presented in Fig. 11 in the case of moisture absorption damage in blade 4. (Similar results are obtained for other damage cases.) The vertical hub load variations are shown for different levels of white noise. The noise amplitude is indicated in percentage of the uncontrolled vibration amplitude, for the damaged rotor. Three cases are simulated: 1, 5, and 10% noise. Although the performance of the controller deteriorates as the noise level is increased, in all simulated cases the controller is able to reduce the vibration amplitude to about the same level as the noise amplitude. The algorithm is robust to the presence of noise in the measurements.

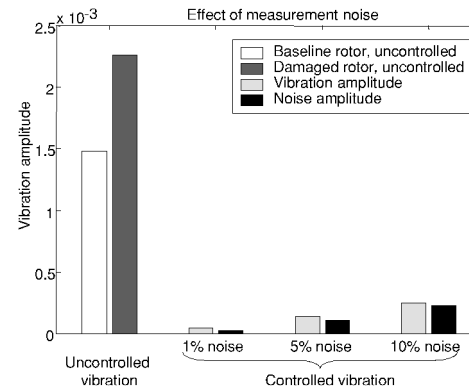

Fig. 11 Effect of measurement noise on vibration reduction with moisture absorption damage in blade 4.

Conclusions

A new real-time adaptive control scheme is developed for helicopter hub vibration reduction using on-blade trailing-edge flaps. This scheme controls each trailing-edge flap independently, taking into account individual blade dissimilarities, while using fixed-frame measurements.

Using numerical simulation, the controller is tested in presence of rotor dissimilarities, modeled by changes in mass, stiffness, and aerodynamic properties of the damaged blade. The controller generates different control inputs for each blade according to their individual dissimilarities and successfully minimizes vibration. Observations from the present study are as follows:

1) The vertical vibration is reduced by 99% in 150 revolutions in all test cases, and in each case the flap requirements do not exceed 2-deg peak-to-peak at $\mu = 0.3$.

2) Simultaneous reduction of three hub loads (vertical shear, pitching moment, and rolling moment) by more than 99% is achieved in less than 150 revolutions with required flap deflections of less than 6 deg peak-to-peak at $\mu = 0.3$.

3) The controller adapts to a change in advance ratio from 0.3 to 0.35 in less than 50 revolutions by generating new control inputs for each flap (5 deg peak-to-peak for $\mu = 0.35$ compared to 3 deg peak-to-peak for $\mu = 0.3$).

4) With noise-corrupted measurements, the present controller reduces the vibration amplitude to about the same level as the noise amplitude. With 10% measurement noise, the vertical vibration is reduced by 89% in amplitude at $\mu = 0.3$.

Future research will use the comprehensive rotor code UMARC for more realistic controller simulations, and the controller behavior will be checked through a smart rotor test in a wind tunnel.

Acknowledgments

The authors gratefully acknowledge the support for this research work provided by the Army Research Office under Grant DAAH-04-96-10334, Technical Monitor Gary Anderson, and The Boeing Company, Technical Monitor Friedrich Straub.

References

[1] Friedmann, P. P., and Millott, T. A., "Vibration Reduction in Rotorcraft Using Active Control: A Comparison of Various Approaches," *Journal of Guidance, Control, and Dynamics*, Vol. 18, No. 4, 1995, pp. 664–673.

[2]Nguyen, K., and Chopra, I., "Application of Higher Harmonic Control to Rotors Operating at High Speed and Thrust," *Journal of the American Helicopter Society*, Vol. 35, No. 3, 1990, pp. 78–89.

[3]Hammond, C. E., "Wind Tunnel Results Showing Rotor Vibratory Loads Reduction Using Higher Harmonic Blade Pitch," *Journal of the American Helicopter Society*, Vol. 28, No. 1, 1983, pp. 10–15.

[4]Shaw, J., Albion, N., Hanker, E. J., and Teal, R. S., "Higher Harmonic Control: Wind Tunnel Demonstration of Fully Effective Vibratory Hub Forces Suppression," *Journal of the American Helicopter Society*, Vol. 34, No. 1, 1989, pp. 14–25.

[5]Nguyen, K., Betzina, M., and Kitaplioglu, C., "Full-Scale Demonstration of Higher Harmonic Control for Noise and Vibration Reduction on the XV-15 Rotor," *Journal of the American Helicopter Society*, Vol. 46, No. 3, 2001, pp. 182–191.

[6]Wood, E. R., Powers, R. W., Cline, C. H., and Hammond, C. E., "On Developing and Flight Testing a Higher Harmonic Control System," *Journal of the American Helicopter Society*, Vol. 30, No. 1, 1985, pp. 3–20.

[7]Ham, N. D., "Helicopter Individual Blade Control and Its Applications," *39th Annual Forum Proceedings*, American Helicopter Society, Alexandria, VA, 1983, pp. 613–623.

[8]Guinn, K. F., "Individual Blade Control Independent of a Swashplate," *Journal of the American Helicopter Society*, Vol. 27, No. 3, 1982, pp. 25–31.

[9]Richter, P., and Blaas, A., "Full Scale Wind Tunnel Investigation of an Individual Blade Control System for the BO-105 Hingeless Rotor," *19th European Rotorcraft Forum Proceedings*, Vol. 19, No. 2, Associazione Italiana di Aeronautica e Astronautica, Rome, 1993, pp. G5-1–G5-12.

[10]Jacklin, S. A., Nguyen, K., Blaas, A., and Richter, P., "Full-Scale Wind Tunnel Test of a Helicopter Individual Blade Control System," *50th Annual Forum Proceedings*, American Helicopter Society, Alexandria, VA, 1994, pp. 579–596.

[11]Chopra, I., "Status of Application of Smart Structures Technology to Rotorcraft Systems," *Journal of the American Helicopter Society*, Vol. 45, No. 4, 2000, pp. 228–252.

[12]Straub, F. K., "A Feasibility Study of Using Smart Materials for Rotor Control," *Smart Materials and Structures*, Vol. 5, No. 1, 1996, pp. 1–10.

[13]Millott, T. A., and Friedmann, P. P., "Vibration Reduction in Helicopter Rotors Using an Active Control Surface Located on the Blade," *Proceedings of the 33rd AIAA/ASME/ASCE/AHS/ASC Structures, Structural Dynamics, and Materials Conference*, AIAA, Washington, DC, 1992, p. 1975.

[14]Milgram, J., and Chopra, I., "Parametric Design Study for Actively Controlled Trailing Edge Flaps," *Journal of the American Helicopter Society*, Vol. 43, No. 2, 1998, pp. 110–120.

[15]Koratkar, N. A., Spencer, M. G., and Chopra, I., "Wind Tunnel Testing of a Mach-Scaled Active Rotor with Trailing-Edge Flaps," *57th Annual Forum Proceedings*, American Helicopter Society, Alexandria, VA, 2001, pp. 1069–1099.

[16]Johnson, W., "Self-Tuning Regulators for Multicyclic Control of Helicopter Vibration," NASA TP 1996, March 1982.

[17]Chopra, I., and McCloud, J. L., "Numerical Simulation Study of Open-Loop, Closed-Loop and Adaptive Multicyclic Control Systems," *Journal of the American Helicopter Society*, Vol. 28, No. 1, 1983, pp. 63–77.

[18]Spencer, M. G., Sanner, R. M., and Chopra, I., "Adaptive Neurocontrol of Simulated Rotor Vibrations Using Trailing Edge Flaps," *Journal of Intelligent Material Systems and Structures*, Vol. 10, No. 11, 2000, pp. 855–871.

[19]Spencer, M. G., Sanner, R. M., and Chopra, I., "Development of Neural Network Controller for Smart Structure Activated Rotor Blades," *Proceedings of the 39th AIAA/ASME/AHS Adaptive Structures Forum*, AIAA, Reston, VA, 1998, pp. 3326–3336.

[20]Spencer, M. G., Sanner, R. M., and Chopra, I., "Adaptive Neurocontroller for Vibration Suppression and Shape Control of a Flexible Beam," *Journal of Intelligent Material Systems and Structures*, Vol. 9, No. 3, 1998, pp. 160–170.

[21]Hauptman, P., *Sensors—Principles and Applications*, Prentice–Hall, Englewood Cliffs, NJ, 1991, pp. 63–65.

[22]McCool, K. M., Flitter, L. A., and Haas, D. J., "Development and Flight Test Evaluation of Rotor System Load Monitoring Technology," *54th Annual Forum Proceedings*, American Helicopter Society, Alexandria, VA, 1998, pp. 408–418.

[23]McKillip, R. M., "An Accelerometer-Based Instrumentation System for Measurement of Helicopter Rotor Motion and Loads," *52nd Annual Forum Proceedings*, American Helicopter Society, Alexandria, VA, 1996, pp. 979–995.

[24]Roget, B., and Chopra, I., "Trailing-Edge Flap Control Methodology for Vibration Reduction of Helicopter with Dissimilar Blades," *Proceedings of the 42nd AIAA/ASME/AHS Adaptive Structures Forum*, AIAA, Reston, VA, 2001, pp. 1877–1887.

[25]Abbot, I. H., and Von Doenhoff, A. E., *Theory of Wing Sections*, Dover, New York, 1959.

[26]Ganguli, R., Chopra, I., and Haas, D. J., "Helicopter Rotor System Health Monitoring Using Numerical Simulation and Neural Networks," *53rd Annual Forum Proceedings*, American Helicopter Society, Alexandria, VA, 1997, pp. 1285–1296.

[27]Koratkar, N., "Smart Helicopter Rotor with Piezoelectric Bender Actuated Trailing-Edge Flaps," Ph.D. Dissertation, Dept. of Aerospace Engineering, Univ. of Maryland, College Park, MD, 2000.